

Effect of oscillation frequency on wall shear stress and pressure drop in a rectangular channel for heat transfer applications

R Blythman¹, T Persoons¹, N Jeffers² and DB Murray¹

¹ Department of Mechanical and Manufacturing Engineering, Trinity College Dublin, Dublin 2, Ireland.

² Thermal Management Research Group, Efficient Energy Transfer (ηET) Department, Bell Labs Research, Alcatel-Lucent Ireland, Blanchardstown Business & Technology Park, Snugborough Rd, Dublin 15, Ireland.

E-mail: blythmar@tcd.ie

Abstract.

The exploitation of flow unsteadiness in microchannels is a potentially useful technique for enhancing cooling of future photonics systems. Pulsation is thought to alter the thickness of the hydrodynamic and thermal boundary layers, and hence affect the overall thermal resistance of the heat sink. While the mechanical and thermal problems are inextricably linked, it is useful to decouple the parameters to better understand the mechanisms underlying any heat transfer enhancement. The current work characterises the behaviour of the wall shear stress and pressure gradient with frequency, using experimental particle image velocimetry (PIV) measurements and the analytical solution for oscillatory flow in a two-dimensional rectangular channel. Both wall shear stress and pressure gradient are augmented with frequency compared to steady flow, though the pressure gradient increases more significantly as a result of growing inertial losses. The three distinct regimes of unsteadiness are shown to display unique relationships between the parameters pertinent to heat transfer and should therefore be considered independently with respect to thermal enhancement capability. To this end, the regime boundaries are estimated at Womersley number $Wo = 1.6$ and 28.4 in a rectangular channel, based on the contribution of viscous and inertial losses.

1. Introduction

Pulsating flow, which has been found to enhance heat transfer by as much as 40% in minichannel heat sinks [1], has been proposed as a key component of the solution for removing the high heat fluxes generated by future generation photonics integrated circuits (PICs) [2]. While the lasers dissipate just 100 mW each, their small volume results in very high, localised heat fluxes to the order of 1 kW/cm^2 . It is thought that the pulsations in a channel flow alter the thickness of the hydrodynamic and thermal boundary layers and reduce the overall thermal resistance. Alternatively, pulsation may create more complex flow structures and mixing effects. It is clear that the relationship between the fluid mechanical and thermal problems plays an important role in the mechanism of augmentation; however, it is often convenient to decouple and characterise the problems independently. Hence, an understanding of the fluid mechanics is relevant for the design and operation of future solutions to heat transfer problems.

The fluid mechanics of unsteady flow were treated mathematically as early as 1851 with Stokes' second problem [3], considering the one-dimensional shear flow of a viscous fluid near a flat plate oscillating in a direction parallel to its length. The historical work found that the flow was inviscid far from the wall, outside of the so-called Stokes boundary layer. The thickness δ of this region varies depending on the relative balance of viscous and inertial flow stresses, given by the dimensionless Womersley number [4], $Wo = (D_h/2)\sqrt{\omega/\nu}$. For significant δ , viscous stresses must be considered in the near-wall region using the solutions to the Navier-Stokes equations. First solved by Sexl [5], a multitude of analytical studies have since followed using several mathematical solution techniques – including Fourier expansion [6], Laplace transform [7] and Green function [8] methods – to analyse the interdependence of the pertinent parameters.

The shear stress at the wall is an important indicator for heat transfer enhancement as it is intrinsically related to the thickness of the hydrodynamic boundary layer. Due to the difficulties associated with measuring near-wall velocities and wall shear stresses using non-intrusive measurement techniques, Zhao and Cheng [9] indirectly calculated the temporal evolution of wall shear stress in a pipe using pressure drop measurements, finding good agreement with theory for a range of values $2.4 \leq Wo \leq 9.9$. Blythman et al. [10] qualitatively studied the near-wall gradients of experimentally-measured pulsating velocity profiles. The results, found to be in good agreement with theory, displayed significant temporal fluctuations of the near-wall velocity gradients, which were dependent on the frequency regime of pulsation. Also, the increase in pressure gradient relative to steady flow, important in practical applications, was theoretically found to vary significantly. The solved magnitude and phase of the pressure gradient, relative to the flow rate, has been confirmed experimentally by Ray et al. [11] for $0.25 \leq Wo \leq 7.93$. Hence, the unique characteristics of each flow regime indicate that the effects of pulsation on heat transfer enhancement and pressure drop should be independently studied.

To define limits to the characteristic flow conditions, Ohmi et al. [12] investigated the behaviour of a collection of four parameters: a couple measuring the relative contributions of the viscous and inertia terms, and the phases of the flow rate and wall shear stress. The boundaries for the pipe geometry were arbitrarily defined at frequencies where the viscous and inertia terms comprised 95% of the overall pressure gradient. Below $Wo = 2.36$, the viscous Stokes layer spans the entire channel and the quasi-steady approximation is valid. Above $Wo = 28$, the flow is inertia-dominated, the Stokes layer is thin, and the assumption of inviscid flow holds in the channel. Ray et al. [11] experimentally investigated the transition in a pulsating pipe flow using a parameter given by the ratio of the flow rate and pressure gradient oscillation amplitudes as well as the phase delay between the variables with the results well corroborated by theory. Haddad et al. [13] expanded the solution to theoretically compare the transition in a parallel plate channel. The amplitude of the varying pressure gradient and the phase shift were found to be higher in a channel flow meaning that transition occurred sooner in the channel according to their criteria; however, the parallel plate channel investigated had twice the hydraulic diameter of the pipe. The transition has not been studied in rectangular channels.

Hence, the aim of the current work is: (i) to analyse the wall shear stress augmentation of oscillatory flow in a quantitative manner to form a basis for future heat transfer studies, (ii) to investigate the pressure drop in terms of viscous and inertial loss contributions to investigate the feasibility of practical application, and (iii) to identify the limits of the quasi-steady, transitional and inertia-dominated regimes in rectangular channels based on the behaviour of these parameters.

2. Analytical solution for oscillating flow

For an oscillating laminar flow with localised and time-dependent velocity $U'(y, z, t)$ in the x direction, the Navier-Stokes equations in Cartesian coordinates are simplified to [3]:

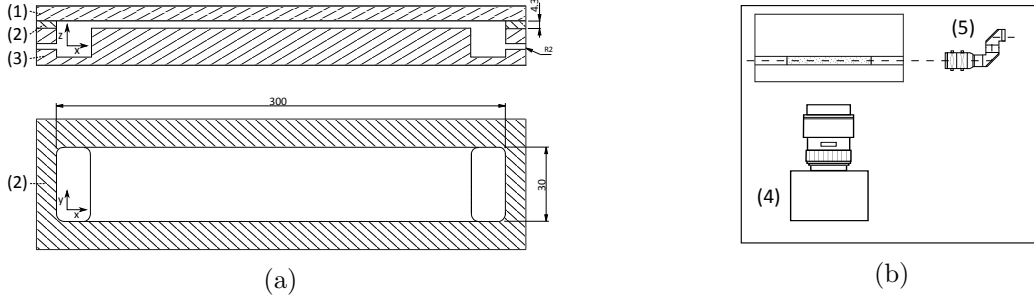


Figure 2: (a) Acrylic test piece containing rectangular channel 300 mm long \times 30 mm wide \times 4.2 mm high, (1) cover plate, (2) channel plate, and (3) base plate with inlet and outlet, (b) Orientation of (4) camera and (5) laser light sheet optics to capture the velocity profile.

$$\nu \nabla^2 U' - \frac{dU'}{dt} = \frac{1}{\rho} \nabla P' \quad (1)$$

where ρ and ν are the density and kinematic viscosity of the fluid, $\nabla^2 = \delta^2/\delta y^2 + \delta^2/\delta z^2$ is the two-dimensional Laplacian operator, and $\nabla P' = dP'/dx$ is the oscillating pressure gradient. The origin is set at the lower left corner of the channel such that $0 \leq y \leq a$ and $0 \leq z \leq b$. Equation 1 may be integrated over a cross-section to give the momentum balance equation:

$$\frac{\Gamma}{A} \cdot \bar{\tau}'_w + \rho \frac{d\bar{U}'}{dt} = \nabla P' \quad (2)$$

where Γ is the perimeter length, $\bar{\tau}'_w$ is the perimeter mean of the wall shear stress and \bar{U}' is the mean velocity. Equation 2 quantifies the pressure drop in a channel, resulting from viscous and inertial contributions. The linearity of Equations 1 and 2 allows the steady and time-dependent components to be decoupled. The Green function for velocity is [8]:

$$G_U(y, z, t) = \frac{16}{\pi^2} \sum_{m=0}^{\infty} \sum_{n=0}^{\infty} \frac{Z}{(2m+1)(2n+1)} \cdot e^{-\nu\beta t} \quad (3)$$

where:

$$Z = \sin \frac{(2m+1)\pi y}{a} \sin \frac{(2n+1)\pi z}{b}; \quad \beta = \frac{\pi^2(2m+1)^2}{a^2} + \frac{\pi^2(2n+1)^2}{b^2} \quad (4)$$

The solution for the local instantaneous time-dependent velocity is attained by convolving G_U with a sinusoidally oscillating accelerative function $f(t) = (1/\rho)\nabla P_t \cdot \cos(\omega t)$:

$$U'(y, z, t) = -\frac{16\nabla P_t}{\rho\pi^2} \sum_{m=0}^{\infty} \sum_{n=0}^{\infty} \frac{Z}{(2m+1)(2n+1)} \cdot \frac{\nu\beta\cos(\omega t) + \omega\sin(\omega t) - \nu\beta e^{-\nu\beta t}}{\nu^2\beta^2 + \omega^2} \quad (5)$$

Solutions for flow rate $Q'(t)$ and cross-sectional flow rate at the channel mid-height $Q'_{cs}(t)$ have been reported in a previous study [10]. ∇P_t is determined using the latter expression with computed integrals of the phase-averaged experimental velocity profiles. Starting from rest, these quantities will contain transients for a period after the motion starts governed by the $e^{-\nu\beta t}$ term, which tends to zero in the steady periodic state. The wall shear stress distribution, at $y = [0, a]$ for example, is determined by $\tau'_{w2}(z, t) = \mu[\delta U'(0, z, t)/\delta y]$:

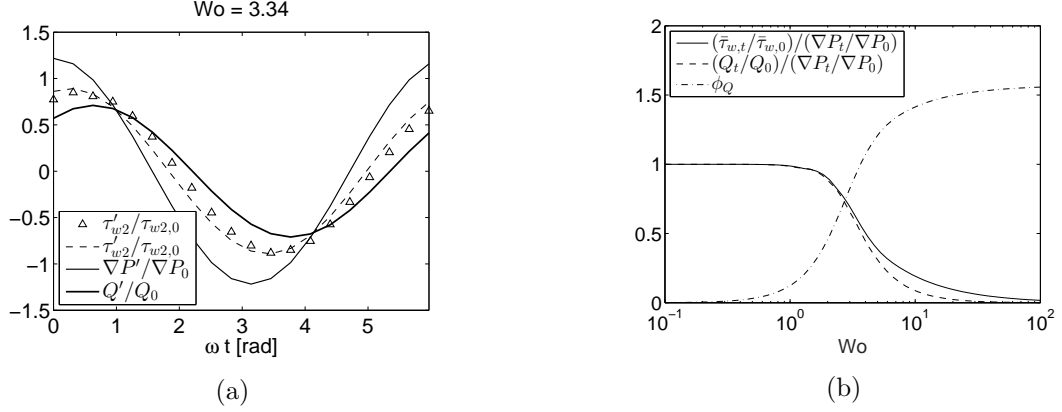


Figure 4: (a) Temporal evolution of $\tau'_{w2}/\tau_{w2,0}$ at channel mid-height, $\nabla P'/\nabla P_0$ and Q'/Q_0 for $Wo = 3.33$, $Q_t/Q_0 = 0.7$, (b) Evolution of amplitudes and phases of $\bar{\tau}'_w/\bar{\tau}_{w,0}$ and Q'/Q_0 with Wo . Lines and symbols represent analytical solutions and experimental measurements respectively.

$$\tau'_{w2}(z, t) = -\frac{16\nu\nabla P_t}{\pi a} \sum_{m=0}^{\infty} \sum_{n=0}^{\infty} \frac{\sin[(2n+1)\pi z/b]}{(2n+1)} \cdot \frac{\nu\beta\cos(\omega t) + \omega\sin(\omega t) - \nu\beta e^{-\nu\beta t}}{\nu^2\beta^2 + \omega^2} \quad (6)$$

The mean value at each wall is $\bar{\tau}'_{w2} = (1/b) \int_0^b \tau'_{w2} dz$. The mean over the entire perimeter $\bar{\tau}'_w$ is the weighted mean of the individual wall averages $\bar{\tau}'_w = (a\bar{\tau}'_{w1} + b\bar{\tau}'_{w2})/(a+b)$.

3. Experimental

3.1. Apparatus

3.1.1. Channel Test Section The test piece consists of a single rectangular channel 300 mm long \times 30 mm wide \times 4.2 mm high laser cut from optically transparent acrylic, covered above and below by acrylic pieces. The inlet and outlet are machined into the base piece, as illustrated in Figure 2(a). Sealing is achieved using silicone rubber gaskets. The viewing window is 75 mm long, centered in the 300 mm length to reduce asymmetrical effects. To facilitate optical access through the narrow edge of the channel plate, the machined surfaces are polished.

3.1.2. Gear Pump Pulsator The flow is driven by a micro annular gear pump (HNP Mikrosysteme mzs-4605, 72 mL/min) and operated using a Terminal Box S-G05 controller and Matlab software. Pulsating flow of a given mean, frequency and amplitude is generated by discretising the corresponding sinusoid into a finite number of time steps. At each interval, a timer function executes and writes a motor speed to the controller based on the phase of the period. A maximum step size of 0.5 s is used to ensure that the inertia of the motor causes a smooth temporal flow rate. A counter implemented in the timer function records the phase of the output flow. At desired phase values, a digital output pin on the motor controller is set to high and sent to the imaging system to trigger image capture.

3.1.3. Particle Image Velocimetry The imaging system uses particle image velocimetry (PIV) to measure the local flow velocities. Collimated green (532 nm) light from a pair of Nd:YAG lasers (15 Hz, 200 mJ per pulse) is focused and diverged using concave and convex lenses (with focal lengths of 1000 mm and -25 mm respectively) to produce a laser plane of about 1 mm thickness. The sheet illuminates the 4 μ m diameter nylon-12 tracer particles (TSI P/N 10084)

with which the fluid is seeded. Images of the flow are captured by a TSI 4 MP (2352 x 1768 pixels) PowerView CCD camera with a close-up Sigma DG 105 mm focal length macro lens, interfaced to the PC using an Xcelera frame grabber. The camera and laser system are aligned at right angles to each other to capture the velocity distribution across the 30 mm channel width, as illustrated in Figure 2(b). System timing is controlled by a Model 610035 LaserPulse Synchroniser. This control unit also reads an external 800 μ s TTL pulse trigger signal from the pump controller to phase-lock measurements to the sinusoidal oscillation of the flow. The entire PIV system is completely controlled by a dedicated computer running TSI's Insight 4G data acquisition software.

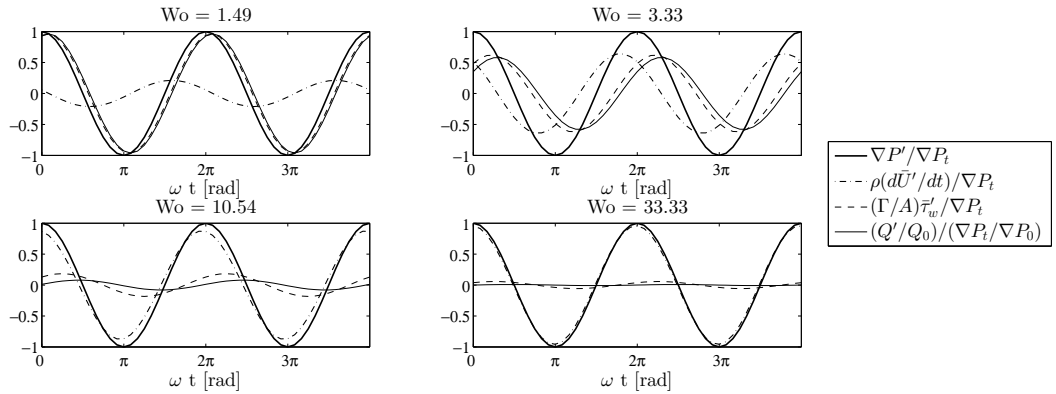


Figure 5: Instantaneous viscous and inertial contributions to the overall pressure gradient for $Wo = 1.49, 3.33, 10.54$ and 33.33 .

4. Results & Discussion

In this section, the experimental and theoretical results for pulsating flows with Reynolds numbers $Re_0 = 34$, $Wo = 1.49, 3.33$ and 10.54 ($f = 0.02, 0.1$ and 1 Hz) are presented. For completeness, pulsations with a very high Womersley number $Wo = 33.33$ ($f = 10$ Hz), which is unachievable with the gear pump pulsator, are studied analytically. The absence of inertia ($d\bar{U}'/dt = 0$) in the steady components of these flows results in a mean pressure drop that is entirely as a result of shear stress at the walls of the channel. Thus, only the oscillating components of the flow are considered, which are computed through subtraction of the mean steady profile solution $Re_0 = 34$ from the pulsating profiles.

4.1. Wall shear stress and pressure gradient

To determine the wall shear stress at the midpoint of the channel height $\tau'_{w2}(b/2, t)$, the slope between the vector nearest the wall ($y = 0.3$ mm) and the wall itself is computed from the velocity data. Plotted by the symbols of Figure 4(a) for the example case of $Wo = 3.33$, these experimental values are in good agreement with that predicted by theory. The pressure gradient and the wall shear stress lead the flow rate by 0.63 and 0.31 radians, respectively. With $\tau'_{w1}(y, t)$ and all but one point on $\tau'_{w2}(z, t)$ unknown, estimation of the overall mean wall shear stress is difficult and analysis is confined to theory.

Figure 4(b) plots the amplitudes and phases of the space-averaged wall shear stress $\bar{\tau}_{w,t}/\bar{\tau}_{w,0}$ and the flow rate Q_t/Q_0 , normalised by the pressure gradient $\nabla P_t/\nabla P_0$, as a function of frequency. The shear stress at the wall is found to increase with frequency compared to quasi-steady oscillations. This is as a result of augmented near-wall velocity gradients, which were observed in a previous study [10] and are depicted for a range of frequencies in Figure 7. However,

the pressure gradient is found to increase more substantially compared to the shear stress, as a consequence of inertial losses in the system (see Section 4.2). Hence, while the enhanced shear rates at high pulsating frequencies may indicate augmented heat transfer, the pressure gradients required to drive these flows are significantly higher than those of steady flows. This trade-off may be measured using the ratio of the increase in wall shear stress relative to that of the pressure drop $(\bar{\tau}_{w,t}/\bar{\tau}_{w,0})/(\nabla P_t/\nabla P_0)$. This pseudo-performance coefficient is plotted in Figure 4(b) with frequency. The flow rate oscillates in phase with the pressure gradient at low frequencies. A phase lag develops at higher frequencies that tends to $\pi/2$ radians.

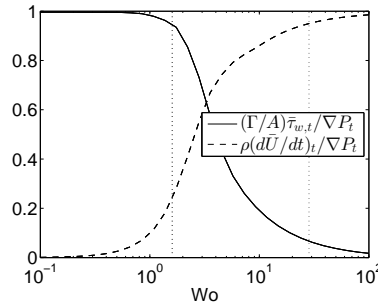


Figure 6: Viscous and inertial stress oscillation amplitudes, normalised by the pressure gradient amplitude, as a function of frequency. Vertical lines delineate the frequency regime boundaries.

4.2. Viscous and inertial stresses

The relationship between the viscous $(\Gamma/A)\bar{\tau}'_w$, inertial $\rho d\bar{U}'/dt$, and pressure gradient $\nabla P'$ terms may be investigated through the momentum integral equation (Equation 2). Figure 5 illustrates that the relative contributions of the individual stresses to the overall pressure drop varies with time for a given frequency, based on the phases and amplitudes of the individual terms. Also plotted are the temporal evolutions of the flow rate oscillations $(Q'/Q_0)/(\nabla P_t/\nabla P_0)$, which always lag the inertial terms by $\pi/2$ radians. The amplitudes of these terms capture the increase in magnitudes of pressure oscillations relative to the flow rate oscillations. For the slowest oscillations, the acceleration of the fluid is negligible and viscous losses dominate. The flow is quasi-steady with the overall pressure gradient oscillating in phase with the viscous stress at the wall of the channel. Further, the flow rate has the same amplitude as and oscillates in phase with the pressure gradient. As the frequency is increased to $Wo = 3.33$, the value of the inertia term becomes appreciable, with an amplitude similar to that of the viscous term. Thus, the flow is in the transitional regime and the resultant phase of the pressure gradient is somewhere between that of the individual contributions. A phase difference appears between the pressure gradient and the flow rate, and $(Q'/Q_0)/(\nabla P_t/\nabla P_0)$ decreases due to the augmented oscillating pressure gradient. At $Wo = 10.54$, the majority (though less than 95%) of losses in the system are caused by inertia and the pressure gradient phase approaches that of the inertial term. Moreover, the phase delay between the driving pressure difference and the flow rate increases and ∇P_t increases further compared to Q' . For $Wo = 33.33$, the pressure drop in the channel is mostly due to and varies in phase with the acceleration of the fluid. The flow is in the inertia-dominated regime with the pressure gradient leading the rate of flow by $\pi/2$ radians.

4.3. Critical points of transition

Ohmi et al. [12] defined boundaries to the various regimes based on adherence to a certain mathematical approximation. With few inertial losses in the system, the flow is quasi-steady. When the majority of the pressure drop is due to inertia, the assumption of inviscid flow

holds. This definition is hence useful for reducing the calculation times of hydrodynamic models in engineering applications. In Figure 6, which plots the amplitudes of viscous and inertial forces relative to that of the pressure gradient as a function of oscillation speed, three unique frequency regimes may be distinguished: the region where the amplitude of the viscous term is approximately the same as that of the pressure gradient, the region where the amplitude of the inertial stress is close to that of the pressure gradient, and the range of frequencies between where the amplitude of both contributing terms are significant. Using 5% limits, the critical frequencies are found to be $Wo = 1.6$ and 28.4 , compared to $Wo = 1.32$ and 28 for pipe flow. Incidentally, it should be noted that the amplitudes of the stress contributors, $\rho(d\bar{U}'/dt)/\nabla P_t$ and $(\Gamma/A)\bar{\tau}'_w/\nabla P_t$, do not necessarily sum to one, as is well illustrated in Figure 5 for $Wo = 3.33$.

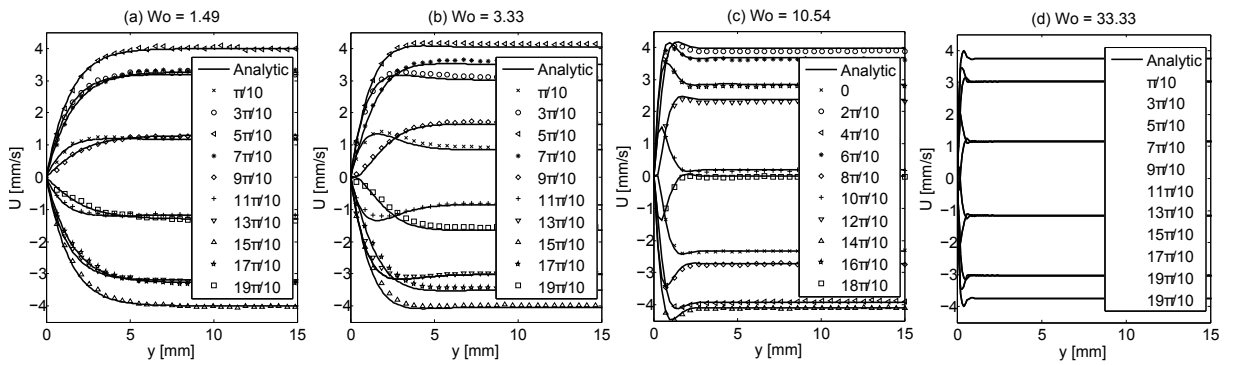


Figure 7: Phase-averaged oscillating velocity profiles for (a) $Wo = 1.49$ ($f = 0.02$ Hz) and $Q_t/Q_0 = 0.7$, (b) $Wo = 3.33$ ($f = 0.1$ Hz) and $Q_t/Q_0 = 0.7$, (c) $Wo = 10.54$ ($f = 1$ Hz) and $Q_t/Q_0 = 1$, and (d) $Wo = 33.33$ ($f = 10$ Hz) and $Q_t/Q_0 = 1$. Solid lines and symbols represent analytical solutions and experimental measurements respectively.

4.4. Velocity Profiles

The evolving relationship between viscous and inertial stresses with frequency results in distinct velocity distributions dependent on the regime of unsteadiness. The unique characteristics predicted, which are apparent in both the experimental and theoretical profiles of Figure 7, owe primarily to the growing phase delays in the system. The quasi-steady profile closely resembles that of steady flow (with some unsteady effects still observable) and local velocity oscillations are universally in phase. With increasing frequency, a lag appears between the main fluid body and the accelerating pressure gradient as discussed in Section 4.1. Near the wall however, viscous stresses reduce the momentum of fluid layers, which are inclined to reverse quickly when the pressure gradient reverses, leading to the observed annular effects of the mid-frequency velocity profiles. The overshoot continues to grow and move closer to the wall. This leads to what is essentially plug flow, as seen in the theoretical inertia-dominated velocity profile.

Figure 7 also portrays the narrowing of the Stokes layer with frequency. The Stokes layer thickness, given by $\delta = 2\pi\sqrt{2\nu/\omega}$ [3], is the distance that vorticity diffuses in one period of oscillation. At higher frequencies, the vorticity has less time to diffuse at the constant speed of viscous diffusion before being annulled by vorticity with opposing sign. At the lowest evaluated frequency, the Stokes layer with $\delta = 22.4$ mm spans the entire cross-section and hence the flow is well-approximated as quasi-steady. At $Wo = 33.3$, the Stokes layer thickness is 1 mm and the assumption of inviscid flow is reasonable. The intermediate frequencies have thicknesses close to the channel's hydraulic diameter, $\delta = 10$ and 3.2 mm respectively, and both viscous and inviscid regions must be considered.

5. Conclusion

This work has investigated the relationship between the pertinent parameters of pulsating flow in a rectangular channel, using near-wall velocity gradients of particle image velocimetry (PIV) measurements and the analytical solution for flow in a two-dimensional rectangular channel solved using the method of Green functions [8]. The behaviour of the wall shear stress and pressure gradient amplitudes with frequency was studied in a quantitative manner to determine the feasibility of superimposed flow unsteadiness in high-end heat transfer applications. Both parameters were found to augment, with the latter growing at a faster rate than the former. Inertial losses were identified as the cause of the high pressure drops, whose overall contribution was also investigated with frequency. Since each flow exhibits unique characteristics that may affect heat transfer, boundaries to the quasi-steady, transitional and inertia-dominated regimes were defined in a rectangular channel using the definition of Ohmi et al. [12], which is based on the adherence of the flow to mechanical models.

In practical applications, it is possible that a trade-off exists where heat transfer enhancement is balanced by increased pressure demands. While the high shear rates of the inertia-dominated regime are desirable, the very large pressure drops are probably unfeasible, especially in microchannels where high frequencies to the order of kHz are required. The ratio of the wall shear stress to the pressure drop augmentation acts as a performance indicator using solely fluid mechanical parameters.

Acknowledgments

The authors would like to acknowledge the financial support of the Irish Research Council (IRC) under grant number EPSPG/2013/618.

References

- [1] T. Persoons, T. Saenen, T. Van Oevelen, and M. Baelmans, "Effect of flow pulsation on the heat transfer performance of a minichannel heat sink," *Journal of Heat Transfer*, vol. 134, no. 9, p. 091702, 2012.
- [2] N. Jeffers, J. Stafford, K. Nolan, B. Donnelly, R. Enright, J. Punch, A. Waddell, L. Erlich, J. O'Connor, A. Sexton, R. Blythman, and D. Hernon, "Microfluidic cooling of photonic integrated circuits (PICs)," in *Fourth European Conference on Microfluidics, Limerick, Ireland*, 2014.
- [3] G. Stokes, *On the effect of the internal friction of fluids on the motion of pendulums*, vol. 9. Pitt Press, 1851.
- [4] J. Womersley, "Method for the calculation of velocity, rate of flow and viscous drag in arteries when the pressure gradient is known," *The Journal of Physiology*, vol. 127, no. 3, pp. 553–563, 1955.
- [5] T. Sexl, "Über den von E.G. Richardson entdeckten annuläreffekt ," *Zeitschrift für Physik*, vol. 61, no. 5-6, pp. 349–362, 1930.
- [6] S. Uchida, "The pulsating viscous flow superposed on the steady laminar motion of incompressible fluid in a circular pipe," *Zeitschrift für angewandte Mathematik und Physik ZAMP*, vol. 7, no. 5, pp. 403–422, 1956.
- [7] H. Ito, "Theory of laminar flow through a pipe with non-steady pressure gradients," *Proceedings of the Institute of High Speed Mechanics*, p. 163, 1953.
- [8] C. Fan and B. Chao, "Unsteady, laminar, incompressible flow through rectangular ducts," *Zeitschrift für angewandte Mathematik und Physik ZAMP*, vol. 16, no. 3, pp. 351–360, 1965.
- [9] T. Zhao and P. Cheng, "The friction coefficient of a fully developed laminar reciprocating flow in a circular pipe," *International Journal of Heat and Fluid Flow*, vol. 17, no. 2, pp. 167–172, 1996.
- [10] R. Blythman, N. Jeffers, T. Persoons, and D. Murray, "Localized and time-resolved velocity measurements of pulsatile flow in a rectangular channel," in *Eighteenth International Conference on Fluid Mechanics and Thermodynamics, Rio de Janeiro, Brazil*, 2016.
- [11] S. Ray, B. Ünsal, F. Durst, Ö. Ertunc, and O. Bayoumi, "Mass flow rate controlled fully developed laminar pulsating pipe flows," *Journal of Fluids Engineering*, vol. 127, no. 3, pp. 405–418, 2005.
- [12] M. Ohmi, M. Iguchi, and T. Usui, "Flow pattern and frictional losses in pulsating pipe flow: Part 5, wall shear stress and flow pattern in a laminar flow," *Bulletin of JSME*, vol. 24, no. 187, pp. 75–81, 1981.
- [13] K. Haddad, Ö. Ertunc, M. Mishra, and A. Delgado, "Pulsating laminar fully developed channel and pipe flows," *Physical Review E*, vol. 81, no. 1, p. 016303, 2010.